Available online at www.sciencedirect.com
SCIENCE DIRECT
Polymer 46 (2005) 4827–4838
polymer
www.elsevier.com/locate/polymer

Finite strain behavior of poly(ethylene terephthalate) (PET) and poly(ethylene terephthalate)-glycol (PETG)

Rebecca B. Dupaix[a,*], Mary C. Boyce[b]

[a]Department of Mechanical Engineering, The Ohio State University, 650 Ackerman Road Suite 255, Columbus, OH 43210, USA
[b]Department of Mechanical Engineering, Massachusetts Institute of Technology, Cambridge, MA 02139, USA

Received 8 October 2004; received in revised form 29 March 2005; accepted 31 March 2005
Available online 22 April 2005

Abstract

Uniaxial and plane strain compression experiments are conducted on amorphous poly(ethylene terephthalate) (PET) and poly(ethylene terephthalate)-glycol (PETG) over a wide range of temperatures (25–110 °C) and strain rates (.005–1.0 s^{-1}). The stress–strain behavior of each material is presented and the results for the two materials are found to be remarkably similar over the investigated range of rates, temperatures, and strain levels. Below the glass transition temperature ($\theta_g = 80$ °C), the materials exhibit a distinct yield stress, followed by strain softening then moderate strain hardening at moderate strain levels and dramatic strain hardening at large strains. Above the glass transition temperature, the stress–strain curves exhibit the classic trends of a rubbery material during loading, albeit with a strong temperature and time dependence. Instead of a distinct yield stress, the curve transitions gradually, or rolls over, to flow. As in the sub-θ_g range, this is followed by moderate strain hardening and stiffening, and subsequent dramatic hardening. The exhibition of dramatic hardening in PETG, a copolymer of PET which does not undergo strain-induced crystallization, indicates that crystallization may not be the source of the dramatic hardening and stiffening in PET and, instead molecular orientation is the primary hardening and stiffening mechanism in both PET and PETG. Indeed, it is only in cases of deformation which result in highly uniaxial network orientation that the stress–strain behavior of PET differs significantly from that of PETG, suggesting the influence of a *meso*-ordered structure or crystallization in these instances. During unloading, PETG exhibits extensive elastic recovery, whereas PET exhibits relatively little recovery, suggesting that crystallization occurs (or continues to develop) after active loading ceases and unloading has commenced, locking in much of the deformation in PET.
© 2005 Elsevier Ltd. All rights reserved.

Keywords: Poly(ethylene terephthalate); Stress–strain behavior; Strain-induced crystallization

1. Introduction

Poly(ethylene terephthalate) (PET) is widely used in many high-volume commercial and consumer applications. Examples include films, fibers, and food containers such as soda bottles. The widespread success of PET in these applications is attributed to its ability to crystallize upon deformation at the temperatures and strain rates used during processing. Strain induced crystallization increases the density of the material, increases its resistance to gas permeability, aids in long term dimensional stability, and imparts anisotropy to the final product. A consequence of anisotropy is increased stiffness and strength of the polymeric product in certain preferential directions. Poly (ethylene terephthalate)-glycol (PETG), a non-crystallizing amorphous copolymer of PET, does not occupy the same industrial niche as PET, precisely because it lacks the ability to undergo strain-induced crystallization. Instead, its uses are directed toward applications involving large, thermo-formed parts, such as point-of-purchase display panels or vending machine faces. PET is not an option in these applications because crystallization during cooling would give the final product an undesirable cloudy, opaque appearance.

As PET continues to be used in manufacturing processes, a cost-motivated need arises for ways to predict material behavior a priori, both in terms of material behavior during processing, as well as end product mechanical behavior. Process simulations enable the prediction of processing parameters (temperatures, pressures, loads, and strain rates)

* Corresponding author. Tel.: +1 614 292 8404; fax: +1 614 292 3163.
E-mail address: dupaix.1@osu.edu (R.B. Dupaix).

0032-3861/$ - see front matter © 2005 Elsevier Ltd. All rights reserved.
doi:10.1016/j.polymer.2005.03.083

required to produce a valid part before costly molds are made or expensive equipment is purchased.

Current models of the deformation behavior of PET under process loading conditions vary both in scope and level of detail. Largely, constitutive models for the finite strain stress–strain behavior of PET are based on curve fits to small sets of data, such as at one strain rate over a small range of temperatures. The validity of these models beyond the initial experimental parameters must be questioned. Particular challenges in modeling include the behavior of polymers at very large deformations, the strong dependence on rate and temperature, and the incorporation of strain-induced crystallization in the models.

This work aims to make progress in some of these areas by better understanding the effects of strain rate, strain state, temperature, and crystallization through mechanical experiments. That understanding can then be applied to developing a constitutive model based on underlying physical mechanisms. By conducting experiments on both PET and non-crystallizing PETG, effects of crystallization on stress–strain behavior can be isolated. Additionally, the data obtained on PETG will be representative of the rate and temperature dependence of amorphous polymers at temperatures ranging from below to above glass transition. Here, uniaxial and plane strain compression experiments have been conducted for these two polymers, with specific emphasis on the temperature region just above the glass transition. Temperature and strain rate were varied to obtain a large sampling of the mechanical behavior of the polymers. Compression experiments allowed for obtaining a uniform sample temperature and for controlling true strain rate during the experiments.

2. Background

2.1. PET

The mechanical behavior of PET has been extensively studied over the years. From early drawing experiments by Marshall and Thompson [1] to modern in situ FTIR and WAXS experiments on PET films (Middleton, et al. [2]), PET has remained a popular research subject. Yet, in spite of the large amount of experimental literature on PET, many aspects of its mechanical behavior remain elusive, in particular the effects of strain-induced crystallization on the stress–strain behavior.[1]

Early experimental work [4] showed that varying the thermal and mechanical history of PET fibers led to significant differences in crystallinity and birefringence. Early theories to explain the mechanical behavior associated strain hardening with crystallization. This theory was unable to capture the behavior of PET fibers, but the idea that crystallization causes strain hardening has endured in work on PET.

Several groups have looked at the effect of annealing after deformation on PET. Misra and Stein [5] conducted experiments on PET drawn near θ_g. Crystallinity, obtained using density, wide angle X-ray diffraction, and small angle light scattering experiments, increased in the deformed material when it was subsequently annealed. A rod-like crystal structure which developed during drawing evolved into spherulites during annealing. Peszkin and Shultz [6] annealed PET fibers at temperatures ranging from 100 to 200 °C and under a small tensile force. They observed through shrinkage and birefringence measurements that a competition existed between chain-recoiling and crystallization. They found that crystallization kinetics increased with higher temperatures and higher tension. Chain orientation also increased with tension.

Rietsch, et al. [7] studied tensile drawing of PET from 20 to 80 °C. Cold drawn PET was observed to neck at a natural draw ratio of 4.3, roughly independent of rate and temperature (rates ranged from 0.05 to 5 cm min^{-1}, gage length was 4.75 mm). Hot drawn PET, however, deformed uniformly. Sweeney, et al. [8] found that necking would occur in PET below 60 °C and would not occur above 80 °C. At intermediate temperatures, necking would occur only at high strain rates, due to the strain-rate dependence of θ_g.

Long and Ward [9,10] looked at tensile drawing and shrinkage force studies on PET. They found that by calculating a network draw ratio, properties of deformed PET could be correlated with different deformation histories. Gordon, et al. [11] also observed that their results from two-stage uniaxial and constant-width stretching of PET could be consistently interpreted using a molecular network model.

Ajji and coworkers [12] performed uniaxial tension experiments on PET films at 80 °C over a range of strain rates and final strains. Post-deformation DSC measurements indicated that crystallinity increased in films drawn beyond a draw ratio of 3.0. At higher strain rates, this critical draw ratio shifted to lower values. Similarly, Dargent, et al. [13] used DSC and X-ray diffraction to measure post-deformation crystallinity in samples deformed at 100 °C and at a strain rate of 0.14 s^{-1}. They observed strain-induced crystallization to occur beyond a critical stretch of 2.8.

Salem [14] investigated rate-dependence of crystallization in hot drawn PET. He concluded from density measurements and wide angle X-ray scattering data that crystallization began at the inflection point in the stress–strain curve and shifted to higher draw ratios and lower stress levels as the strain rate decreased. He also observed that crystallite size increased with draw ratio, crystallite sizes ranging from 2.5 to 4.0 nm. Clauss and Salem [15] observed that in PET drawn uniaxially at 90 °C orientation developed more quickly at higher strain rates.

Jabarin [16] measured birefringence after biaxial stretching of PET. Results showed that molecular orientation and

[1] For a more thorough literature review on PET, see Dupaix [3].

mechanical properties of the drawn films were a strong function of strain rate, final strain, molecular weight, and draw temperature. For a given rate and final strain level, birefringence decreased with increasing temperature. Cakmak, et al. [17,18] also biaxially stretched PET films above θ_g to look at orientation and crystallinity. They observed that crystallinity increased with increasing final stretch and with annealing. The crystal structure was also perfected during annealing. They found that in order to attain the same level of molecular orientation at 100 °C as at 80 °C, the sample had to be stretched further. Le Bourvellec, et al. [19,20] conducted similar experiments, and found that crystallinity and crystallization kinetics depended on the degree of molecular orientation, i.e. PET deformed at higher temperatures crystallized more slowly due to the fact that more molecular relaxation had occurred.

Chandran and Jabarin [21] conducted a large series of experiments in which PET was biaxially stretched both sequentially and simultaneously. Experimental data was reported for a variety of temperatures and strain rates. Similar experiments were performed by Gohil and Salem [22]. They observed differences between sequentially versus simultaneously stretched films, specifically that after a stretch of 2.7 in the second stretch direction, sequentially stretched chains began to realign in that direction. Adams, et al. [23] conducted biaxial stretching experiments on PET over a range of temperatures to compare the behavior of PET in equibiaxial extension and constant-width extension.

Tassin, Vigny and coworkers [24,25] performed sequential biaxial stretching experiments on PET followed by annealing. They found that crystallinity increased with an increase in draw ratio and that crystallization appeared at lower draw ratios for lower temperatures. (All experiments were above θ_g.) Also, the chain axes were found to be more highly aligned with increasing draw ratio or decreasing temperature. Upon subsequent stretching in the transverse direction, the crystals rotated toward the transverse direction.

Salem [26] looked at the difference between tensile tests at constant extension rate and those at constant strain rate. He observed that crystallization onset occurred at shorter times and that crystallization rate was higher for constant strain rate experiments. Additional constant-force and constant-extension rate experiments on PET [27,28] led to the conclusion that at higher overall rates, the material will acquire higher molecular orientation and lower crystallinity. Lower draw temperature produced the same result.

Guan, et al. [29,30] compared biaxial stretching with uniaxial compression of PET. In compression PET developed more planar orientation and more strain induced crystallization than in biaxial stretching, however in both experiments the draw rate was held constant, so in extension the strain rate decreased during the experiment and in compression the strain rate increased.

Compression experiments have also been used to look at deformation in PET. Zaroulis and Boyce [31] focused on the glassy regime up to θ_g. They conducted both uniaxial compression and plane strain compression experiments over a range of strain rates. Work by Llana and Boyce [32] continued this effort by adding substantial experimental results above θ_g. They also used WAXD and DSC to look at crystallization as a function of temperature, rate, and strain state. Their experiments were from 90 to 105 °C and at strain rates from -0.005 to $-2.0\ s^{-1}$. They observed a sequence of four characteristic features in the stress–strain behavior: (1) a relatively high initial stiffness, (2) a roll-over to flow, (3) an increase in stress with continuing strain, (4) a dramatic increase in stress at high strains. Each depended strongly on strain rate, temperature, and strain state. Crystallinity, measured in deformed specimens after unloading and cooling, increased with increasing strain rate and decreasing deformation temperature in both uniaxial and plane strain compression.

In 1996, one group began investigating the theory that strain-induced crystallization occurs during drawing. Blundell and coworkers [2,33,34] published results of uniaxial tension tests on PET in which X-ray patterns were recorded during deformation. Results of their early work [33,34] indicated that strain-induced crystallization did not occur during drawing, but was postponed until the moment when deformation stopped. These tests were conducted at temperatures ranging from 80 to 140 °C and at nominal strain rates of 10 and $13\ s^{-1}$. They suggested that the crystallization which previous researchers had measured actually occurred once active stretching ceased. Subsequently, they have clarified their results with experiments conducted at 80 and 85 °C over a range of nominal strain rates ($0.001–0.7\ s^{-1}$) [2]. From these results, they have shown that crystallization can occur during deformation at lower strain rates, with more crystallization occurring during drawing at low strain rates than at high strain rates. They hypothesize that at the very high strain rates seen in industrial processes, no crystallization would occur during drawing. In all cases, experiments were limited to uniaxial tension. Using the same technique, Schrauwen, et al. [35] obtained data showing that PET did not crystallize during uniaxial drawing at room temperature.

Gorlier, et al. [36] performed video-controlled, constant strain rate tensile experiments on PET. They observed that crystallinity developed much more rapidly when the samples were quenched more slowly. They proposed that crystallization was not directly related to strain hardening but rather to the development of a mesophase. Cole, et al. [37] investigated the morphology of amorphous, drawn (at 80 °C and $2\ cm\ min^{-1}$) and quenched, and drawn and annealed (at 100–200 °C) PET. Results suggested that there is an intermediate stage of the material which is highly ordered, but not as closely packed as in the crystalline material.

The experimental literature on PET illustrates the scientific interest in its behavior. A wide range of experimental techniques have been used to understand

how thermal and mechanical history affect molecular orientation and crystallinity in PET. In each experimental approach, challenges arise in trying to quench a sample quickly enough to remove the effects of the brief annealing after deformation. Recent work involving simultaneous stretching and X-ray measurements has attempted to address this.

2.2. PETG

Another polymer of less fame is an amorphous copolymer of PET, often called PETG. The letter G refers to the additional glycol group along the backbone of the copolymerizing agent, poly(1,4-cyclohexylenedimethylene terephthalate) (PCT). Specifically, PETG is a random copolymer consisting of 31 mol% PCT and 69 mol% PET. PET and PETG both exhibit quite similar deformation behavior, have a similar glass transition temperature, and are visually nearly indistinguishable. Yet there is one substantial difference: PET readily undergoes strain-induced crystallization, whereas crystallization is nearly impossible to achieve in PETG at processing temperatures.

Recent work by Kattan, et al. [38] addressed the difference in crystallizability between the two polymers. They conducted uniaxial tension experiments on both materials at a strain rate of $0.14\ s^{-1}$ and a temperature of 95 °C. After deformation, samples were air quenched, following which DSC and X-ray diffraction were used to determine percent crystallinity. They found that very small levels of crystallinity (less than 3%) were attainable in PETG under normal drawing conditions. Upon annealing, it was possible to increase this level of crystallinity, but it was still substantially lower than that of PET. In their follow-up study comparing PET with PETG [39], they observed that upon deformation both materials developed a significant amount of what they called a rigid amorphous phase (35 and 25% in PET and PETG, respectively). This rigid amorphous phase was identified using thermally stimulated depolarisation current experiments. After the formation of the rigid amorphous mesophase PET proceeded to crystallize whereas PETG did not (measured crystallinities were 40% for PET and 3% for PETG).

Relatively little additional literature has been published on PETG. Papadopoulou and Kalfoglou [40] found PET and PETG to be completely miscible at all concentrations. They also observed that annealing the blends caused the PET to crystallize and led to embrittlement.

Work by Chen, et al. [41,42] looked at secondary relaxation, impact strength, and yield behavior of a series of polyester copolymer glasses, including PETG. They found that room temperature yield stress decreased as percent PCT increased. The craze stress, on the other hand, increased as percent PCT increased. The tradeoff of yield stress decreasing and craze stress increasing led to a brittle–ductile transition.

As has been discussed, the deformation behavior and morphological structure of PET have been widely studied. Constitutive models have advanced to be able to capture many of the features of the finite strain behavior of PET, but in many instances the incorporation of strain-induced crystallization into the models is highly empirical, and possibly inappropriate due to evidence that at many strain rates the material is not able to crystallize while the deformation is proceeding. At the same time, very little has been published on the mechanical behavior of PETG, and no constitutive models have been proposed to model the deformation behavior of PETG.

3. Material

The material used in all experiments was supplied by Eastman Chemical Co. in the form of 4 in. by 4 in. injection molded plaques of 1/8 in. nominal thickness, from which compression specimens were machined. PETG 6763 with a weight average molecular weight of 38,888 and a polydispersity of 2 and PET 9921 with a weight average molecular weight of 51,365 and a polydispersity of 2 were used for all experiments. Prior to testing, the materials were stored at ambient conditions.[2]

Differential scanning calorimetry (DSC) was performed using a Perkin–Elmer DSC 7 at a constant heating rate of 10 °C/min. The equipment was calibrated with zinc and indium. DSC scans performed on the as-received PETG and PET as well as on deformed PETG indicated that there was no crystallinity in either material before testing nor after testing for PETG. DSC scans also identified the glass transition temperature for both materials as 80 °C.

Dynamic mechanical analysis (DMA) was performed on the as-received PETG material. Specimens were cut using a Buehler Isomet cutoff saw at a very low cutting speed so as to prevent aging of the material. Specimens were approximately 30 mm long, 3.2 mm wide, and 1 mm thick. Each sample was tested in a tensile mode at frequencies ranging from 1 to 100 Hz and at temperatures ranging from 40 to 110 °C. The oscillating force had a mean value of 30 gf (.2943 N) with an amplitude of oscillation of 45 gf (.4415 N). The modulus data for PETG is shown in Fig. 1. The shift in the curve with frequency demonstrates a strain rate dependence of the glass transition temperature. When the material is deformed at higher frequencies, which corresponds to higher strain rates, the glass transition temperature shifts to higher temperatures.

[2] Room temperature (approximately 20 °C) and indoor humidity. All experiments were conducted in the same season, such that relative humidity, though not measured, varied little over the course of the experiments. The very high repeatability and consistency in the data further suggests that humidity fluctuations minimally affected the data.

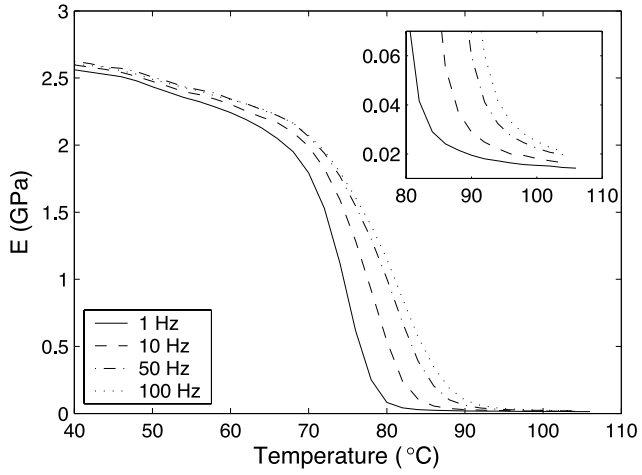

Fig. 1. PETG DMA data. Inset shows enlarged detail at high temperature.

4. Compression tests

4.1. Testing procedure

Two types of compression tests were performed: uniaxial and plane strain. Schematics of the two loading configurations are shown in Fig. 2 along with photographs showing undeformed PETG specimens and specimens deformed at room temperature to a final strain of 1.2. For the uniaxial tests, specimens were cut into circular disks 12.39 mm in diameter. For the plane strain experiments, square cross-section samples were cut to measure 9.55 mm on a side. The thickness of each specimen was that of the plaque thickness, nominally 1/8 in. (3.2 mm). For each test, WD-40, a common lubricant, was applied to the compression platens and a sheet of teflon was placed between the compression platens and the polymer sample to eliminate the effects of friction. Care was taken so that no lubricant contacted the test specimens. The specimens were brought to test temperature by use of an electric resistance heater. They were allowed to come to thermal equilibrium for a total of 20 min.

The compression experiments were performed using an Instron 1350 with servo-hydraulic controls. The cross head speed was controlled using a personal computer running Windows NT and LabView. During uniaxial compression tests, the specimen height was monitored during deformation using an extensometer, thus eliminating load train compliance error. This measurement was also used as feedback to the actuator to provide constant true (logarithmic) strain rate loading conditions. Specimens were compressed at strain rates ranging from -0.005 to $-1.0\ s^{-1}$ to final strains ranging from -1.3 to -2.0 in the uniaxial experiments. True stress was determined by assuming no volume change for the polymer.

Plane strain compression tests were conducted using a channel die placed between the compression platens. This fixture adds a compliance to the load train. This compliance was accounted for when reducing the plane strain data. Plane strain compression results were obtained to strains of -1.3 (largest strain achievable in this setup) at rates ranging from -0.005 to $-1.0\ s^{-1}$.

Temperatures were varied from 25 to 110 °C. In uniaxial compression experiments, temperature was measured using four thermocouples cemented to the compression platens. In plane strain compression experiments, temperature was measured using a single thermocouple in contact with the specimen. A simple computer program monitored the temperature readings from the thermocouples and adjusted the voltage supplied to the furnace to keep the specimen temperature constant during the tests.

4.2. PETG experiments

The results from compression tests on PETG are shown in Figs. 3–13 and are discussed below. Figs. 3–7 show

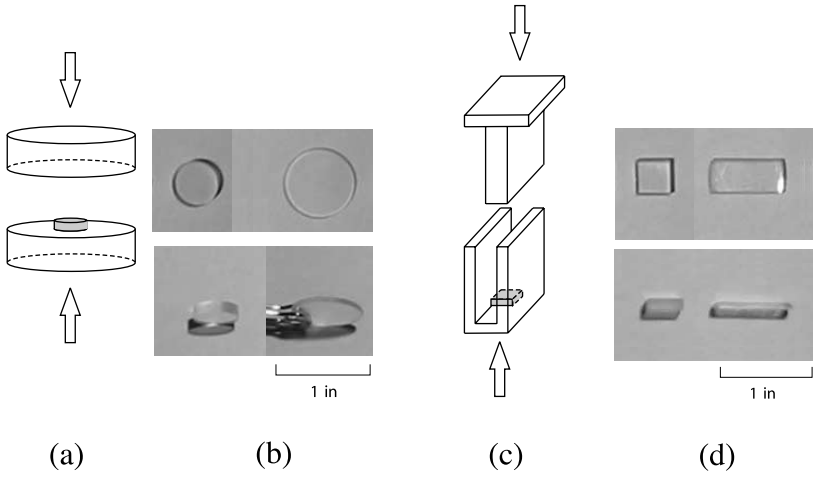

Fig. 2. (a) Uniaxial compression experimental setup (b) uniaxial compression specimen undeformed and deformed (c) plane strain compression experimental setup (d) plane strain compression specimen undeformed and deformed.

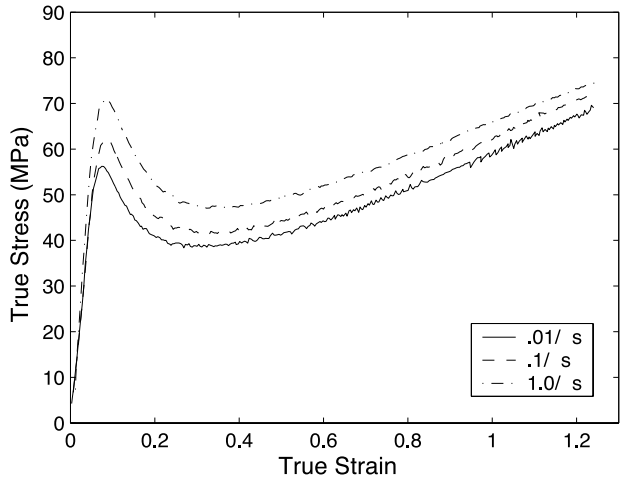

Fig. 3. PETG uniaxial compression data, temperature = 25 °C.

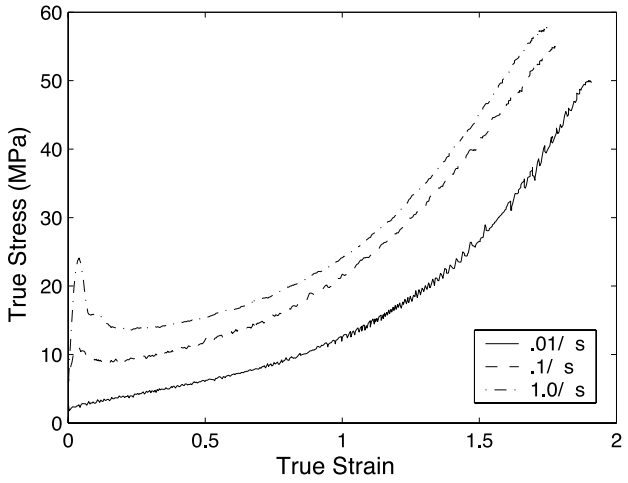

Fig. 5. PETG uniaxial compression data, temperature = 80 °C.

uniaxial compression data at each temperature. Fig. 8 shows the effect of temperature on specimens deformed at $-0.5\ s^{-1}$.

From these figures it can be observed that PETG exhibits the following general trends. First, the material has an initially stiff response which is highly temperature dependent. The modulus decreases moderately with increasing temperature but is fairly independent of strain-rate at temperatures below the glass transition temperature (θ_g). In the transition region, the modulus drops dramatically with increasing temperature. This drop-off occurs at higher temperatures for specimens deformed at higher strain rates. At temperatures above the transition region, the modulus continues to drop as temperature rises, but the change is more moderate. The dependence is also mildly strain-rate dependent above θ_g, with increasing strain rate leading to increased modulus.

Second, at temperatures below the glass transition temperature the polymer exhibits a definite yield stress which increases with increasing strain rate and with decreasing temperature. Yield is followed by a considerable amount of strain softening. The amount of strain softening is relatively strain-rate independent.

At temperatures above the transition temperature, the stress–strain curves show a monotonic rise in stress with increasing strain, which is characteristic of rubber elastomers. The yield stress is no longer abrupt and instead the stress–strain curve gently rolls over and the material begins to flow at a stress level on the order of 1–2 MPa. The magnitude of this flow stress also depends on strain rate and temperature. At higher temperatures and lower strain rates the roll over occurs at lower stress levels. The insets of Figs. 6 and 7 show an enlarged view of the initial modulus and roll over to flow for PETG above the glass transition temperature.

The 80 °C data in Fig. 5 clearly demonstrates the strain rate dependence of the glass transition temperature. Strain rate dependence causes the glass transition temperature to increase with increasing strain rate. At high strain rates, 80 °C is directly in the glass transition region, and the

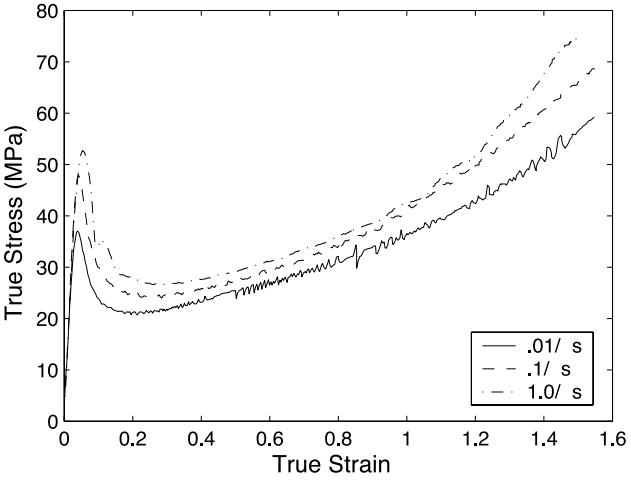

Fig. 4. PETG uniaxial compression data, temperature = 60 °C.

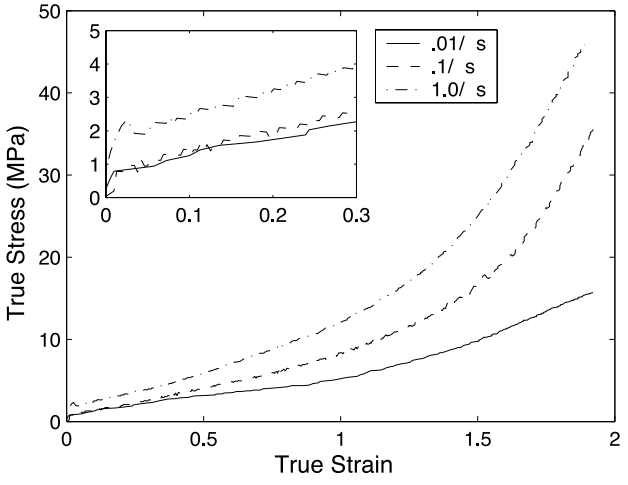

Fig. 6. PETG uniaxial compression data, temperature = 90 °C.

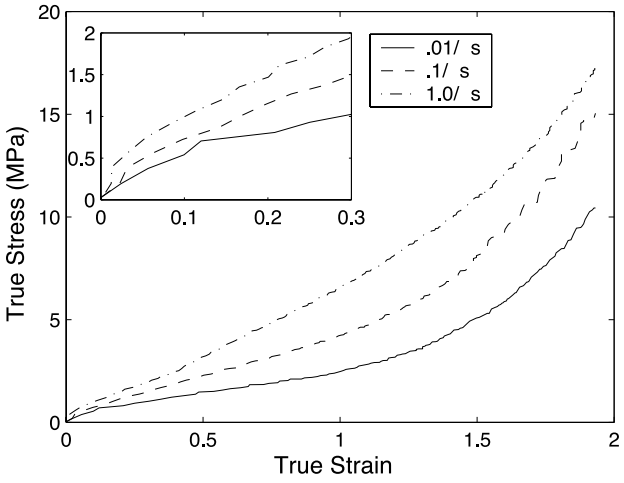

Fig. 7. PETG uniaxial compression data, temperature = 100 °C.

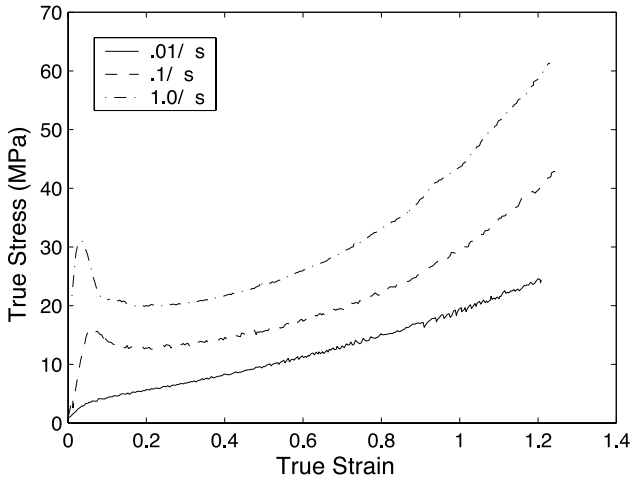

Fig. 9. PETG plane strain compression data, temperature = 80 °C.

material exhibits a clear yield stress and strain softening typical of polymers in the glassy state. As the strain rate decreases, however, the apparent yield stress disappears and the stress–strain curve begins to rise monotonically. This indicates that at lower strain rates the polymer is already above its glass transition at 80 °C and hence exhibits rubbery polymeric behavior.

Third, after the strain softening region (or after the roll over to flow for tests above the transition temperature), the polymer begins to strain harden as the strain level is increased. Strain hardening is evident through an initial hardening modulus in the flow region at moderate strains followed by a dramatic upturn in the stress–strain curve at very large strains. Strain hardening is more pronounced at lower temperatures and higher strain rates. Additionally, with increasing temperature and decreasing strain rate, the strain level at which dramatic strain hardening occurs is postponed to higher strains.

In Fig. 8 the temperature dependence of the material is depicted. At each strain rate, the initial yield or initial flow stress decreases as temperature increases. The hardening slope decreases and the strain level at which the dramatic upswing in stress occurs is greater at higher temperatures. Each of the observed trends is consistent with trends exhibited by PET in compression [31,32].

Figs. 9 and 10 show plane strain compression data at 80 and 90 °C. The plane strain compression data exhibits the same trends as were observed in uniaxial compression. In Figs. 11–13 plane strain and uniaxial deformation are compared. These figures demonstrate that in plane strain compression, the material begins to undergo dramatic strain hardening at a lower strain level than in uniaxial compression.

Effects of adiabatic heating due to plastic deformation can also become significant, particularly at temperatures below the glass transition. This is present in both uniaxial compression and plane strain compression at low temperatures, but is more pronounced in plane strain due to higher stress levels in the material. In the room temperature data of Fig. 11, thermal softening is seen to cause the $-0.5\ s^{-1}$ plane strain curve nearly to cross over the $-0.005\ s^{-1}$ curve at large strains. In the absence of thermal softening,

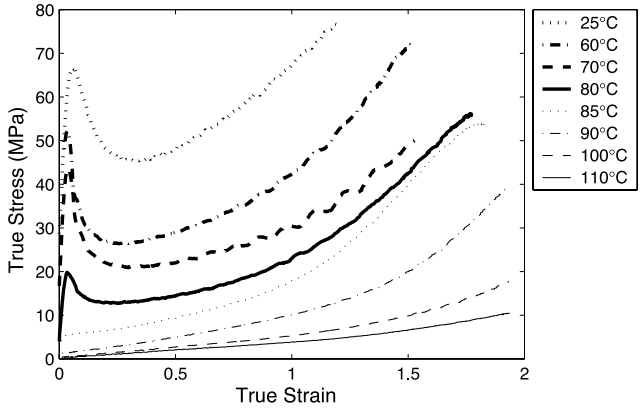

Fig. 8. PETG uniaxial compression data, $\dot{\varepsilon} = -.5/s$.

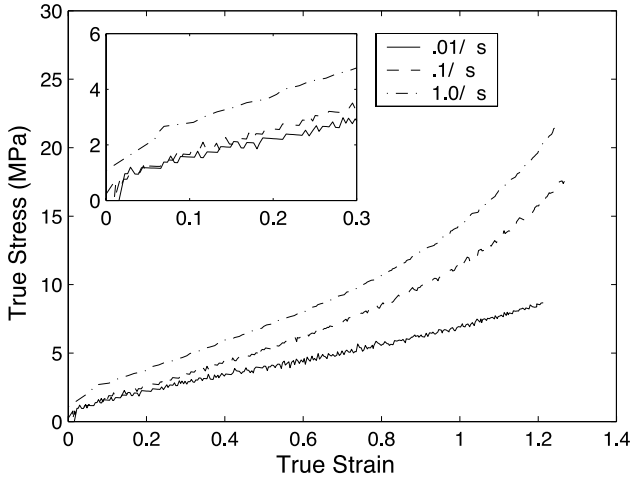

Fig. 10. PETG plane strain compression data, temperature = 90 °C.

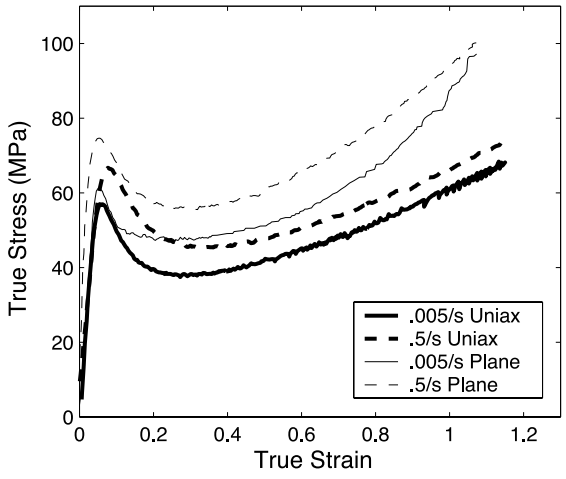

Fig. 11. PETG uniaxial and plane strain compression data, temperature = 25 °C.

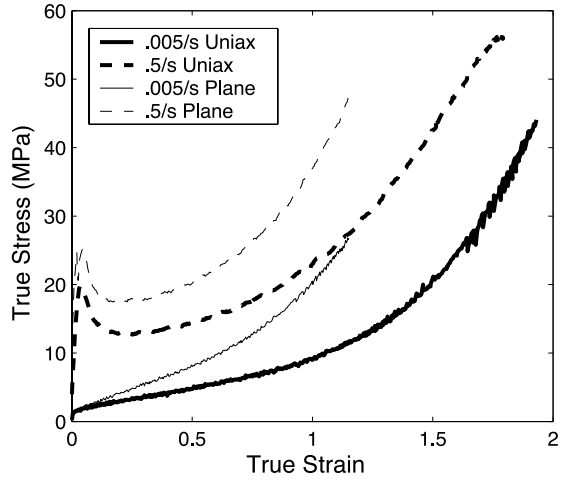

Fig. 12. PETG uniaxial and plane strain compression data, temperature = 80 °C.

the higher rate data would be expected to sustain a higher stress level throughout the deformation.[3]

To summarize the behavior of PETG in compression, the material exhibits four characteristic regions above the glass transition temperature: (1) a relatively stiff initial modulus, (2) a roll-over to flow at around 2 MPa, (3) a gradual stiffening through the moderate strain regime, and (4) a

[3] Due to the inelastic nature of the deformation, heat is generated during the tests. During the longer low strain rate tests the heat is able to dissipate, but during shorter high rate tests, it will not be able to dissipate, but instead cause a temperature rise in the material. As in Zaroulis [31] and Llana [32], each test can be classified as isothermal, adiabatic, or thermomechanically coupled by comparing the time for the experiment (t_{exp}) with the time for heat to transfer out of the specimen ($t_{cond} = (h_i/2)^2/(2k/\rho c)$), where h_i is the specimen height, $k = 0.218$ W m K^{-1} is thermal conductivity, $\rho = 1.330$ g cm^{-3} is the density of amorphous PET, and $c = 1300$ J kg K^{-1} is the specific heat capacity. Using this approach, the experiments at $\dot{\varepsilon} = -0.005$ and -0.01 s^{-1} are determined to be isothermal and experiments at strain rates up to and including -1.0 s^{-1} are thermomechanically coupled.

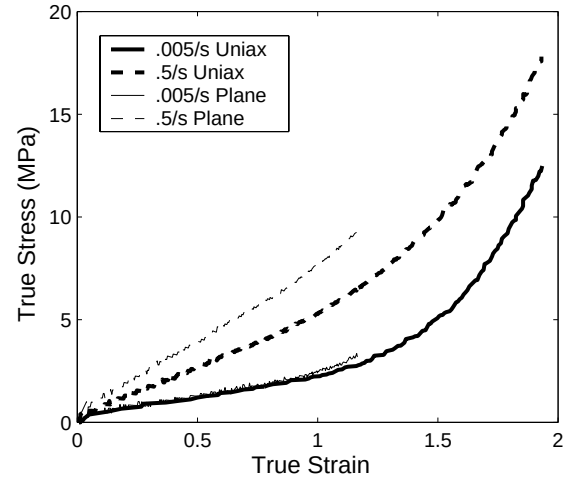

Fig. 13. PETG uniaxial and plane strain compression data, temperature = 100 °C.

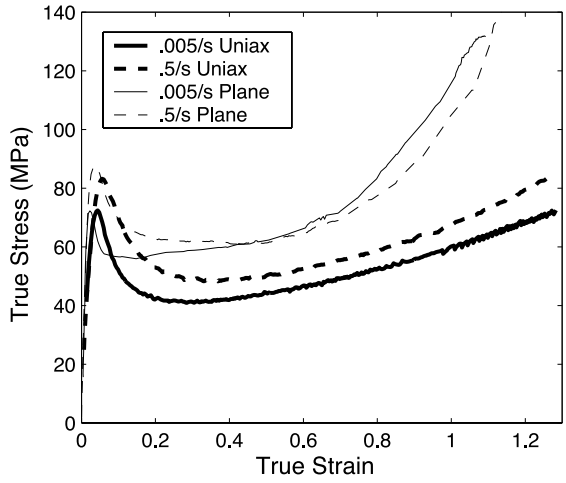

Fig. 14. PET uniaxial and plane strain compression data, temperature = 25 °C.

dramatic upturn in strain at very large strain levels. Each of these features depends strongly on the temperature and rate of deformation. The initial modulus, flow stress, and initial hardening modulus all increase with decreasing temperature or increasing strain rate. The dramatic upturn in strain occurs at earlier strain levels with increasing strain rate or decreasing temperature. The material also exhibits a stiffer response and an earlier upturn in the stress–strain curve in plane strain compression than in uniaxial compression.

4.3. PET experiments

The results of PET compression tests are shown in Figs. 14–17 and are discussed below. From these figures it can be observed that PET exhibits the same general trends as PETG. First, the material has an initially stiff response which is highly temperature dependent, decreasing moderately with increasing temperature below and above the glass

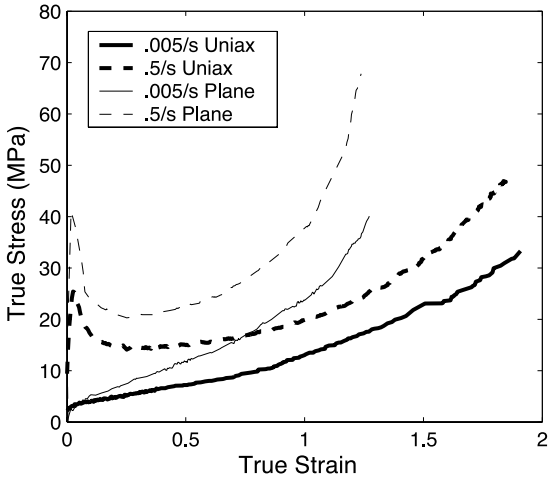

Fig. 15. PET uniaxial and plane strain compression data, temperature = 80 °C.

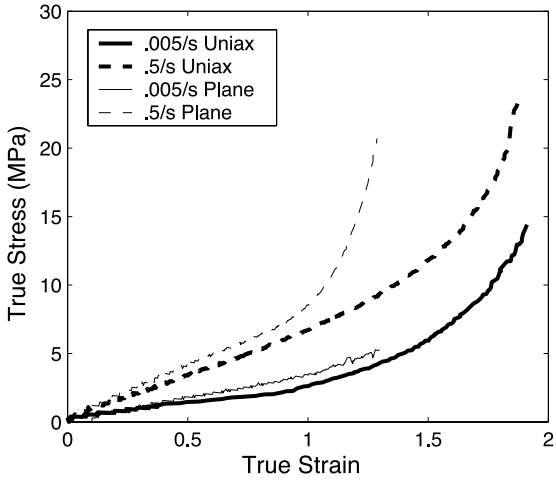

Fig. 17. PET uniaxial and plane strain compression data, temperature = 100 °C.

transition temperature and dropping dramatically with temperature in the transition region. There is also a strong strain rate dependence in the transition region, with increasing strain rate leading to a higher effective θ_g.

Second, at temperatures below the glass transition temperature the polymer exhibits a definite yield stress followed by strain softening. At temperatures above θ_g, the stress–strain curves show a monotonic rise in stress with increasing strain. The magnitude of the yield and flow stresses depends on strain rate and temperature. At higher temperatures and lower strain rates, yield (flow) occurs at lower stress levels. Third, the polymer begins to strain harden as the strain level is increased. The material exhibits both an initial hardening modulus and a dramatic upturn in stress at very large strains. The hardening slope decreases with increasing temperature and the strain at which the dramatic upswing in stress occurs is greater at higher temperatures.

The same trends are observed in both uniaxial and plane strain compression data. Figs. 14–16, in particular, demonstrate that the deformation behavior of PET includes a very dramatic upswing in plane strain compression. This upswing is more pronounced than in uniaxial compression and more dramatic than the behavior shown by PETG (recall Figs. 11 and 12). This is possibly due to either the influence of a *meso*-ordered structure and/or strain-induced crystallization. While strain-induced crystallization is observed in PET in post-deformation samples regardless of the strain state, in plane strain the polymer chains (and crystallites) become preferentially aligned in one direction. In uniaxial compression, on the other hand, the crystallites develop a planar orientation. Figs. 18 and 19 illustrate schematically the development of this different degree of order between the two deformation modes. Fig. 18 draws conceptually on the Arruda-Boyce 8-chain model [43] to illustrate how in uniaxial compression the polymer chains become preferentially aligned within a plane, and in plane strain compression, the chains become preferentially axially aligned. Fig. 19 illustrates the effect this has on final crystal orientation, where the crystal chain axes will follow the molecular orientation. This could explain why the plane strain data hardens so dramatically. In PETG, where strain-induced crystallization does not occur, this dramatic hardening is not seen in plane strain compression.[4]

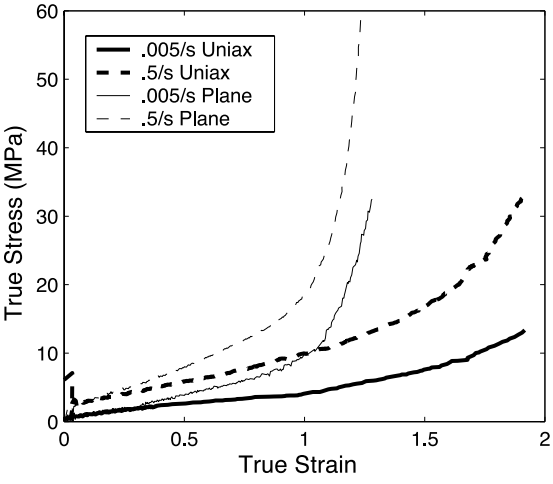

Fig. 16. PET uniaxial and plane strain compression data, temperature = 90 °C.

To summarize the behavior of PET in compression, the material exhibits the same four characteristic regions above the glass transition temperature: (1) a relatively stiff initial modulus, (2) a roll-over to flow at around 2 MPa, (3) a

[4] In situ experiments to measure the development of strain induced crystallization during deformation have only been conducted on uniaxial tension samples (roughly an equivalent deformation mode to plane strain compression). In their most recent experiments, Blundell, et al. [33] found that crystallization could occur during deformation at strain rates similar to those used here. However, no in situ experiments have been reported for biaxial deformation modes similar to the uniaxial compression tests used here.

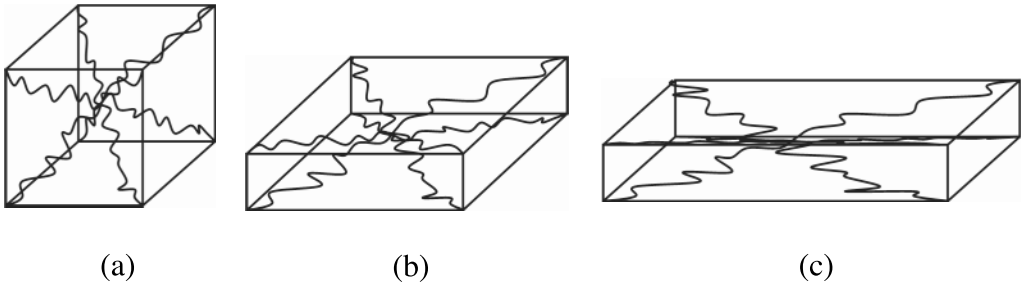

Fig. 18. Schematic showing 8-chain model (a) before deformation (b) after uniaxial compression, and (c) after plane strain compression.

gradual stiffening through the moderate strain regime, and (4) a dramatic upturn in strain at very large strain levels. Each of these features depends strongly on the temperature and rate of deformation. The initial modulus, flow stress, and initial hardening modulus all increase with decreasing temperature or increasing strain rate. The dramatic upturn in strain occurs at earlier strain levels with increasing strain rate or decreasing temperature. The material also exhibits a stiffer response and an earlier upturn in the stress–strain curve in plane strain compression than in uniaxial compression.

5. Comparison of PET and PETG behavior

Careful comparison of the data for PETG with the data for PET show that the overall mechanical behavior of PET and PETG is quite similar. Both materials exhibit all four stress–strain features and have similar dependencies on temperature, strain rate, and strain state. By comparing Figs. 6, 10, and 16 a similar dependence on strain rate is observed for the two materials. With an increase in strain rate, both materials exhibit a stiffer initial modulus, higher flow stress, increased strain hardening, and an earlier dramatic upturn in the stress–strain curve. Similar comparison of Figs. 8 and 14–17 show the temperature dependence of the behavior in the two materials. With increasing temperature, both materials exhibit a decrease in initial modulus and flow stress, less strain hardening, and the dramatic strain hardening is postponed to higher strain levels. Figs. 11–17 also show the state of strain dependence of PETG and PET. In both materials, the response of the material is stiffer in plane strain compression than in uniaxial compression. In PET there is a more dramatic increase in the strain hardening in plane strain compression. This is especially visible in the 90 °C data (Fig. 16). This is likely due to strain-induced crystallization or to the development of a highly ordered mesophase which is able to occur in PET, but not in PETG. Otherwise, the stress–strain behavior of the two materials is nearly identical. Fig. 20 highlights these key similarities and differences.

Although the unloading behavior was not quantified in this work, the PETG exhibited extensive elastic recovery upon unloading above the glass transition. The PET, on the

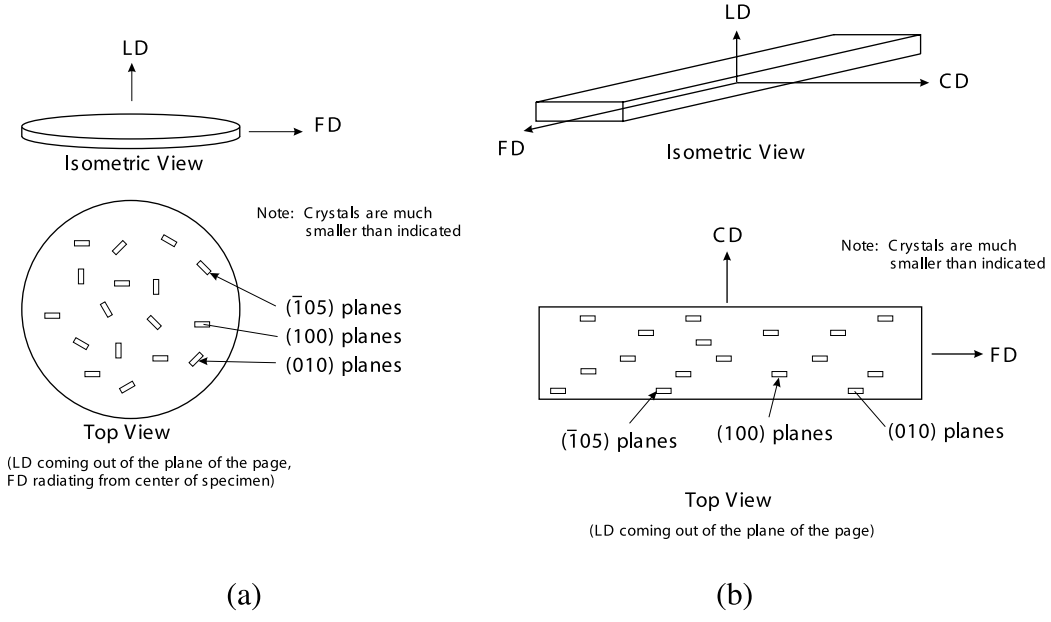

Fig. 19. Orientation of crystals in (a) uniaxial and (b) plane strain compression (from Llana and Boyce [32]).

	Increasing strain rate	Increasing temperature	In plane strain compression
Similarities			
Initial modulus	increases	decreases	increases compared to uniaxial compression
Flow stress	increases	decreases	increases compared to uniaxial compression
Strain hardening	increases	decreases	increases compared to uniaxial compression
Dramatic hardening	shifts to lower strains	shifts to higher strains	shifts to lower strains compared to uniaxial compression
Differences			
Dramatic hardening			more pronounced in PET than PETG

Fig. 20. Key similarities and differences in the mechanical behavior of PET and PETG.

other hand, exhibited very little recovery upon unloading. This suggests that any crystallization that occurred during unloading in the PET served to lock in the deformed state. The lack of crystallization in PETG prevented locking in of the deformed state.

6. Conclusions and future work

The experimental results for PETG contained in this paper should serve as a useful benchmark for developing constitutive models for PETG, enabling simulations of PETG processes. A comparison of the behavior of PET and PETG shows little difference during uniaxial and plane strain compression tests. Differences are only seen in plane strain deformation, where PET exhibits a more dramatic upturn in stress, especially at 90 °C. The overall similarity in the mechanical behavior of the materials suggests that strain-induced crystallization plays almost no role in most deformation conditions, and only influences the mechanical behavior during loading at the very largest strain levels in strain states that give rise to nearly uniaxial molecular orientation of the polymer structure. In these cases, strain induced crystallization may begin at very large strains and continue after deformation has ceased.

Future work will address developing a constitutive model for PETG. This model will then be modified to incorporate strain-induced crystallization in order to capture the differences in behavior of PET at very large stretches and upon unloading.

Acknowledgements

The authors thank Eastman Chemical Co. for supplying materials and financial support and the National Science Foundation for fellowship funding. The authors especially thank Dr T. Pecorini and Dr F. Colhoun of Eastman for helpful discussions. This work made use ofMRSEC Shared Facilities supported by the National Science Foundation, under Award Number DMR-9400334.

References

[1] Marshall I, Thompson AB. The drawing of 'Terylene'. J Appl Chem 1954;4:145–53.
[2] Middleton AC, Duckett RA, Ward IM, Mahendrasingam A, Martin C. Real-time FTIR and WAXS studies of drawing behavior of poly(ethylene terephthalate) films. J Appl Polym Sci 2001;79: 1825–37.
[3] Dupaix RB, Temperature and rate dependent finite strain behavior of poly(ethylene terephthalate) and poly(ethylene terephthalate)-glycol above the glass transition temperature, PhD Thesis, MIT; 2003.
[4] Thompson AB. Strain-induced crystallization in polyethylene terephthalate. J Polym Sci 1959;34:741–60.
[5] Misra A, Stein RS. Stress-induced crystallization of poly(ethylene terephthalate). J Polym Sci: Polym Phys Ed 1979;17:235–57.
[6] Peszkin PN, Schultz IM. Kinetics of fiber heat treatment. II. Poly(ethylene terephthalate) fibers. J Polym Sci: Part B: Polym Phys 1986;24:2591–616.
[7] Rietsch F, Duckett RA, Ward IM. Tensile drawing behavior of poly(ethylene terephthalate). Polymer 1979;20:1133–42.
[8] Sweeney J, Shirataki H, Unwin AP, Ward IM. Application of a necking criterion to PET fibers in tension. J Appl Polym Sci 1999;74: 3331–41.
[9] Long SD, Ward IM. Shrinkage force studies of oriented polyethylene terephthalate. J Appl Polym Sci 1991;42:1921–9.
[10] Long SD, Ward IM. Tensile drawing behaviour of polyethylene terephthalate. J Appl Polym Sci 1991;42:1911–20.
[11] Gordon DH, Duckett RA, Ward IM. A studyt of uniaxial and constant width drawing of poly(ethylene terephthalate). Polymer 1994;35(12): 2554–9.
[12] Ajji A, Guevremont J, Cole KC, Dumoulin MM. Orientation, mechanical, and thermal characterization of drawn PET. Annual technical conference—ANTEC, conference proceedings 1994. p. 1421–3.
[13] Dargent E, Grenet J, Auvray X. Thermal behaviour of drawn semi-crystalline poly(ethylene terephthalate) films. J Therm Anal 1994;41: 1409–15.
[14] Salem DR. Development of crystalline order during hot-drawing of poly(ethylene terephthalate) film: influence of strain rate. Polymer 1992;33(15):3182–8.
[15] Clauss B, Salem DR. A chain-intrinsic fluorescence study of orientation-strain behavior in uniaxially drawn poly(ethylene terephthalate) film. Macromolecules 1995;28:8328–33.
[16] Jabarin SA. Orientation studies of poly(ethylene terephthalate). Polym Eng Sci 1984;24(5):376–84.
[17] Cakmak M, White JL, Spruiell JE. Structural characterization of crystallinity and crystalline orientation in simultaneously biaxially stretched and annealed polyethylene terephthalate films. J Polym Eng 1986;6:291–312.
[18] Cakmak M, Spruiell JE, White JL, Lin JS. Small angle and wide angle

X-ray pole figure studies on simultaneous biaxially stretched poly(ethylene terephthalate) (PET) films. Polym Eng Sci 1987; 27(12):893–905.

[19] LeBourvellec G, Monnerie L, Jarry JP. Amorphous orientation and induced crystallization in uniaxially stretched poly(ethylene terephthalate glycol). Polymer 1986;27:856–60.

[20] LeBourvellec G, Monnerie L, Jarry JP. Kinetics of induced crystallization during stretching and annealing of poly(ethylene terephthalate) films. Polymer 1987;28:1712–6.

[21] Chandran P, Jabarin S. Biaxial orientation of poly(ethylene terephthalate). Part I. Nature of the stress–strain curves. Adv Polym Technol 1993;12(2):119–32.

[22] Gohil RM, Salem DR. Orientation distribution in the noncrystalline regions of biaxially drawn poly(ethylene terephthalate) film: a chain-intrinsic fluorescence study. J Appl Polym Sci 1993;47:1989–98.

[23] Adams AM, Buckley CP, Jones DP. Biaxial hot drawing of poly(ethylene terephthalate): measurements and modelling of strain-stiffening. Polymer 2000;41(2):771–86.

[24] Tassin J, Vigny M, Veyrat D. Biaxial stretching of PET films: a molecular description. Macromol Symp 1999;147:209–20.

[25] Vigny M, Tassin JF, Lorentz G. Study of the molecular structure of pet films obtained by an inverse stretching process. Part 2. Crystalline reorganization during longitudinal drawing. Polymer 1999;40: 397–406.

[26] Salem DR. Crystallization during hot-drawing of poly(ethylene terephthalate) film: influence of the deformation mode. Polymer 1995;36(18):3605–8.

[27] Salem DR. Microstructure development during constant-force drawing of poly(ethylene terephthalate) film. Polymer 1998;39(26): 7067–77.

[28] Salem DR. Orientation and crystallization in poly(ethylene terephthalate) during drawing at high temperatures and strain rates. Polym Eng Sci 1999;39(12):2419–30.

[29] Guan JY, Saraf RF, Porter RS. Evaluation of free and hydrostatic equibiaxial deformation of poly(ethylene terephthalate) by trirefringence measurement. J Appl Polym Sci 1987;33:1517–23.

[30] Guan JY, Wang L, Porter RS. Planar deformation of amorphous poly(ethylene terephthalate) by stretching and forging. J Polym Sci: Part B: Polym Phys 1992;30(7):387–91.

[31] Zaroulis JS, Boyce MC. Temperature, strain rate, and strain state dependence of the evolution in mechanical behaviour and structure of poly(ethylene terephthalate) with finite strain deformation. Polymer 1997;38(6):1303–15.

[32] Llana PG, Boyce MC. Finite strain behavior of poly(ethylene terephthalate) above the glass transition temperature. Polymer 1999; 40(24):6729–51.

[33] Blundell DJ, MacKerron DH, Fuller W, Mahendrasingam A, Martin C, Oldman RJ, et al. Characterization of strain-induced crystallization of poly(ethylene terephthalate) at fast draw rates using synchrotron radiation. Polymer 1996;37(15):3303–11.

[34] Mahendrasingam A, Martin C, Fuller W, Blundell DJ, Oldman RJ, Harvie JL, et al. Effect of draw ratio and temperature on the strain-induced crystallization of poly(ethylene terephthalate) at fast draw rates. Polymer 1999;40(20):5553–65.

[35] Schrauwen BAG, Rastogi S, Govaert LE, Meijer HEH. Wide- and small-angle X-ray scattering studies on the deformation behaviour of PET. 11th International conference on deformation, yield and fracture of polymers. Cambridge UK: Churchill College; 2000. p. 367–70.

[36] Gorlier E, Haudin JM, Billon N. Strain-induced crystallization in bulk amorphous PET under uniaxial loading. Polymer 2001;42:9541–9.

[37] Cole KC, Ajji A, Pellerin E. New insights into the development of ordered structure in poly(ethylene terephthalate). 1. Results from external reflection infrared spectroscopy. Macromolecules 2002; 35(3):770–84.

[38] Kattan M, Dargent E, Ledru J, Grenet J. Strain-induced crystallization in uniaxially drawn PETG plates. J Appl Polym Sci 2001;81:3405–12.

[39] Kattan M, Dargent E, Grenet J. Three phase model in drawn thermoplastic polyesters: comparison of differential scanning calorimetry and thermally stimulated depolarisation current experiments. Polymer 2002;43(4):1399–405.

[40] Papadopoulou CP, Kalfoglou NK. Compatibility behavior of blends of poly(ethylene terephthalate) with an amorphous copolyester. Polymer 1997;38(3):631–7.

[41] Chen LP, Yee AF, Goetz JM, Schaefer J. Molecular structure effects on the secondary relaxation and impact strength of a series of polyester copolymer glasses. Macromolecules 1998;31:5371–82.

[42] Chen LP, Yee AF, Moskala EJ. The molecular basis for the relationship between the secondary relaxation and mechanical properties of a series of polyester copolymer glasses. Macromolecules 1999;32:5944–55.

[43] Arruda EM, Boyce MC. A three-dimensional constitutive model for the large stretch behavior of rubber elastic materials. J Mech Phys Solids 1993;41(2):389–412.